Investigation of latest generation pulsed fiber laser in dissimilar joining of Al and Mg alloys

Qiong Gao (高 琼)[1], Sonia Meco[2], Kehong Wang (王克鸿)[1],*, Qi Zhou (周 琦)[1],
Shun Guo (郭 顺)[1], and Supriyo Ganguly[2]

[1]*School of Material Science and Engineering, Nanjing University of Science and Technology, Nanjing 210094, China*
[2]*Welding Engineering and Laser Processing Centre, Cranfield University, Bedford MK43 0AL, United Kingdom*
Corresponding author: wkh1602@163.com

Dissimilar metal joining of magnesium to aluminum was investigated using the latest generation nanosecond pulsed fiber laser. The tensile shear test shows that the average tensile shear strength of a joint was 86 MPa, which was 75% of the aluminum substrate. The weld interface exhibited a mixture phase (Mg solid solution and $Mg_{17}Al_{12}$) that improves the strength and toughness of the joint. A thin Mg–Al intermetallic compound layer was formed on both sides of the weld seam toward the Al side. Fracture occurred toward the Al substrate side rather than the Mg–Al interface, indicating a high joining strength at the weld interface.

OCIS codes: 140.3390, 140.7090, 140.3538, 160.3900.
doi: 10.3788/COL201816.061401.

The joining of dissimilar materials such as aluminum (Al) and magnesium (Mg) is of high interest for lightweight aerospace and automotive industries, bringing advantages for weight reduction and energy savings[1–3]. However, it is still a challenge to produce reliable Mg–Al joints. The major issue when welding dissimilar Mg/Al alloys is the formation of Al_3Mg_2 and $Mg_{17}Al_{12}$ intermetallic compounds (IMCs) in a large quantity, which have a detrimental effect on joint strength[4,5]. Other issues are their different physical properties (e.g., thermal expansion, conductivity) and the limited mutual solid solubility of Mg and Al[6–8]. Previous studies have been carried out with the goal of understanding and controlling the growth of Mg–Al IMCs[9–14]. It is well known that the Mg–Al reaction depends on the overall transient thermal cycle during joint formation. For this reason, it is important to control the process energy and minimize the welding heat input and cooling time[15].

Nanosecond pulsed laser processing with short pulse duration is extremely popular for fabrication of thin structural alloys[16–20] due to several outstanding advantages when processing, e.g., minimization of the heat-affected zone (HAZ), sharp laser density, and accurate positioning of the heat source, which are important for processing selectivity and the possibility of processing high conductivity materials. All these advantages come from the combination of the following characteristics of the nanosecond pulsed lasers: high peak power, short pulse duration, and very small spot sizes. Such characteristics have the potential of preventing the formation of brittle IMCs and minimizing the HAZ in dissimilar metal joining. Therefore, application of such a laser is promising for forming robust joining between Mg and Al alloys even though in the electronic industry its use has rarely been reported. The present study focuses on the application of such a joining process in thin magnesium to aluminum alloys in autogenous mode

and overlap configuration. The microstructure and metallurgical phase formation were discussed and correlated with the mechanical properties of the joints.

Sheets of 1050 aluminum (0.5 mm × 30 mm × 105 mm) and AZ31B magnesium (1 mm × 30 mm × 105 mm) were used as base materials. The typical chemical compositions of the base metals are provided in Table 1. A G4 nanosecond pulsed fiber laser with 100 W of average output power, 1.06 μm of wavelength, and 35.5 μm of spot diameter at the focus position was used throughout this work. The maximum peak power and energy per pulse are 10 kW and 1 mJ, respectively. The short pulse width ranges from 37 to 500 ns. The surfaces of the base materials were ground and degreased prior to welding. The Al sheet was positioned on top of the Mg sheet in a full overlap joint configuration. A clamping device was developed to ensure no macroscopic gap between the upper and lower sheets [Fig. 1(a)]. The weld area was shielded with pure shield argon gas with a 20 L · min⁻¹ flow rate. The welding parameters were described as follows: peak power 10 kW, travel speed 30 mm/s, short pulse frequency 100 kHz, and pulse width 280 ns. No filler metal was used in the experiment.

Micrographs of welded cross sections were observed by a scanning electron microscope (SEM) in backscattered mode. The SEM is equipped with an energy dispersive spectrometer (EDS). According to ISO 14273:2001 standards, three straight lined test samples were cut with the following dimensions: 30 mm wide and 175 mm long. The mechanical strength of the specimens was measured with a tensile testing machine with a crosshead speed of 0.5 mm/min at room temperature. The shearing tensile strength of the sample is defined as the ratio of the average maximum force obtained from the test to the cross-sectional area of the fracture. As the strength of the joints produced with a single weld seam was too low due to the small width of the weld, 13 parallel weld lines with 0.2 mm

Table 1. Chemical Compositions (%, Mass Fraction) of AZ31B and 1050 Alloys

Material	Al	Zn	Mn	Si	Fe	Cu	Ca	Cr	Mg	Other
AZ31B	2.5-3.5	0.6-1.4	0.2	0.1	0.005	0.05	0.04	—	Bal	0.3
1050	Bal	0.050	0.05	0.25	0.4	0.05	—	—	0.05	0.15
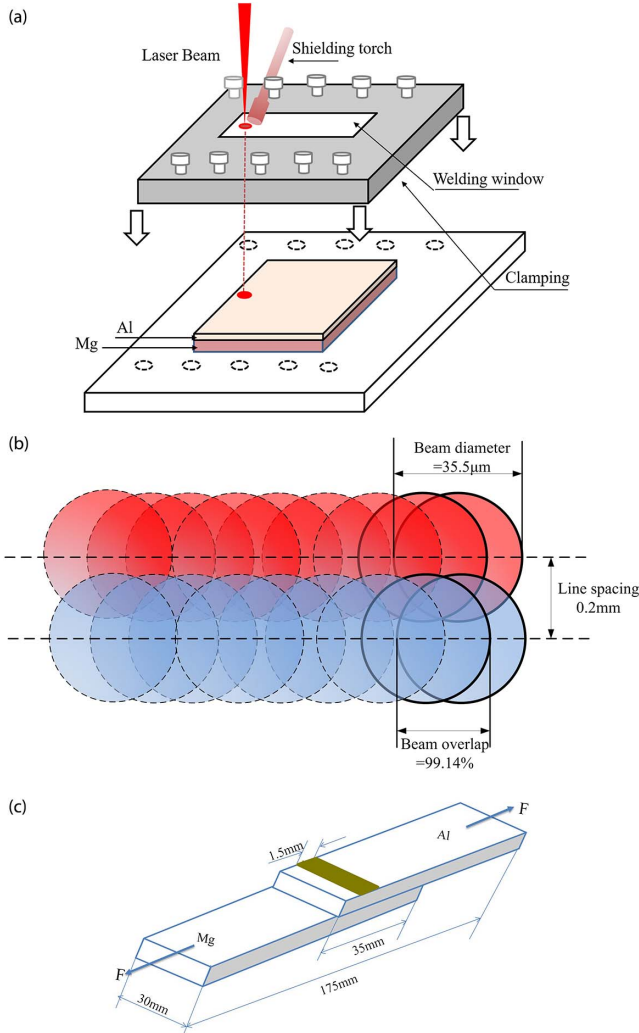
Fig. 1. (a) Schematic representation of the experimental setup; (b) an illustration of the line scanning distance and beam overlap; (c) an illustration of the tensile test sample.

spacing rate [see Fig. 1(b)] were created on each tensile shear sample [Fig. 1(c)] using a laser beam deflective unit from Raylase, which is controlled by the weld MARK 3 software. The adjacent beam overlap factor (δ) is defined as the ratio of the spot diameter (D) and pulse frequency (F) to the travel speed (TS), as shown in Eq. (1):

$$\delta = 1 - \frac{D \times F}{\text{TS}}. \tag{1}$$

It should be noted that 13 parallel line weld samples were only dedicated to tensile tests, not including

microstructure observation. Thanks to the high speed and low heat input, the cooling rate after each weld is fast so that the previous weld heat accumulation has little effect on the following pass. The microstructure of the 13 parallel-line weld is not discussed in this Letter. In this text, the typical microstructure of the one-pass welded sample was investigated. After the mechanical tests, the fracture surfaces of the joints were observed under the SEM.

Figure 2 (a) shows a backscattered micrograph of a one-pass Mg–Al joint. Although some small-scale pores could be observed there is no sign of any visible crack, denoting that the joint was welded successfully in this process. Figure 2(b) shows the spatial distribution of Al and Mg along the weld seam and associated area around the weld. It can be seen that the Mg element diffused into the Al side to form a rich-Mg region near the joint interface. However, the Al element rarely diffused into the Mg side. One possible reason could be the low vaporization temperature of the Mg alloy combined with the nature of the nanosecond pulsed laser welding process. To join 0.5 mm thick Al to 1.0 mm thick Mg, more than a single laser pulse is required because the energy per pulse is only 1 mJ, which is not enough to create a deep weld. The overlapping required in this work was about 99.14%, which means that in each pulse the molten metal is pushed upward inside the keyhole[21]. The EDS mapping shows that part of the Mg was found along the two sides of the weld on the Al side, as indicated by the circle in Fig. 2(b). The microstructural characteristic of the schematically drawn circle in Fig. 2(b) is shown in Fig. 2(c). Compositional and phase analysis (Table 2) shows that this part is composed mainly of cellular dendritic structure composed of an α-Al solid solution and Al_3Mg_2 phases.

During Mg/Al dissimilar metals joining, the interfacial morphology is an important strength-determining factor[22]. To identify whether the interface forms a metallurgical reaction layer, the interfacial morphology was observed by SEM. Figure 3(a) presents the SEM image of the interface of the Mg–Al joint. A thin white transition layer was observed along the two sides of the weld seam on the
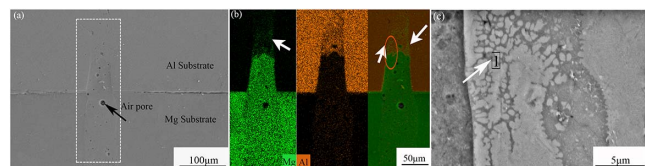

Fig. 2. (a) SEM picture of the cross section of the weld seam; (b) an EDS mapping picture of the weld seam; (c) a micrograph with a higher magnification of the zone indicated in (b).

Table 2. Composition (%, Atomic Fraction) of the Phases Indicated in Figs. 2(c) and 3(b)

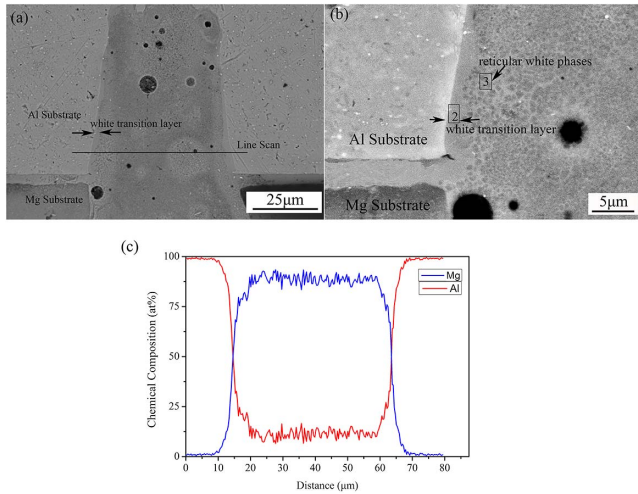| Point	Mg	Al	Possible Phases
1	37	63	α-Al solid solution and Al_3Mg_2
2	52	48	$Mg_{17}Al_{12}$ and Al_3Mg_2
3	80	20	β-Mg solid solution and $Mg_{17}Al_{12}$

Fig. 3. (a) Microstructure of the weld seam; (b) magnified morphology of the weld seam; (c) the line scanning result.

Al side. The magnified image of the transition layer is shown in Fig. 3(b). Continuous white phases (point 2) were located close to the Al substrate side. According to the EDS results (Table 2) and the Mg–Al binary phase diagram (Fig. 4), the atomic ratio of Mg to Al is 1:1, indicating that the continuous white phases are Mg–Al IMCs. Point 3 shows that reticular white phases were deposited on the gray matrix, which is regarded as a Mg solid solution and $Mg_{17}Al_{12}$, according to EDS analysis. EDS line analysis was performed, and the results are shown
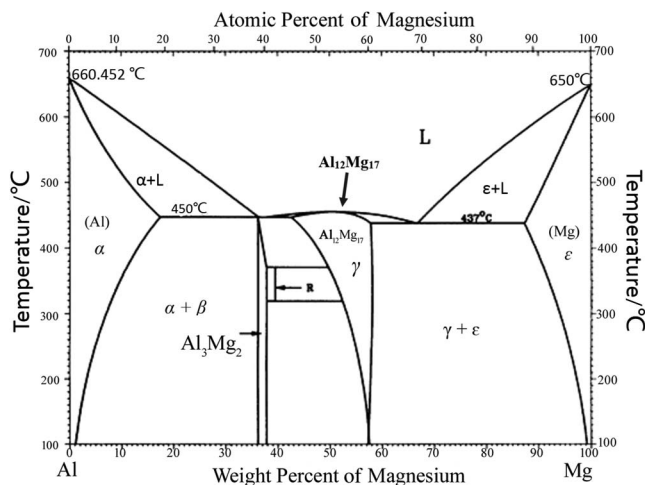
in Fig. 3(c). It is clear that Mg diffused upward to the Al side. Along both sides of the weld seam, the atomic ratio of Mg and Al is 1:1, indicating the formation of Mg–Al IMCs. The concentration pattern of Mg and Al elements in the middle of the weld seam was assumed as a stable step where Mg solid solution formed. These results indicate that no Mg–Al IMCs interlayer is formed in the interface of the joint. Some studies on Mg/Al joining reported that Mg–Al IMCs layer can be observed at the joint interface in laser welding, friction stir welding (FSW), and brazing bonding[23–25], but the reaction layer was not observed in nanosecond pulsed laser welding. The weld interface exhibited a mixture phase composed of Mg solid solution and $Mg_{17}Al_{12}$ IMCs. The reason for that is the fast processing speed used during the nanosecond pulsed laser welding, which allows extremely rapid cooling of the weld seams. Therefore, there is no time for the formation and growing of IMCs.

Figure 5(a) shows the tensile shear test results obtained from dissimilar Mg–Al lap joints and tensile test results from the base metals, 1050 Al, and AZ31B alloys. The sketch of the tensile test samples of the Mg and Al substrates is also shown in Fig. 5(a). The maximum force obtained from the test was 1294 N. The joint failure occurred in the aluminum substrate so that the cross section of the aluminum substrate is regarded as a stressed area (0.5 mm × 30 mm). Therefore, the tensile shear strength of the Mg–Al joint can reach up to 86 MPa, which is 75% of the Al ultimate tensile strength. A typical macroscopic image of the failed lap tensile sample from the Mg–Al joint is shown in Fig. 5(b). The joint failure occurred roughly in the aluminum substrate rather than at the Mg–Al interface. As discussed above, along the two sides of the weld seam the microstructure is mainly composed of Mg–Al IMCs, which are brittle and have low ductility. Therefore, these zones are the weakest of the joint and may be the crack initiation point. However, the dimension of the Mg–Al IMCs layer is approximately 2 μm, which is very

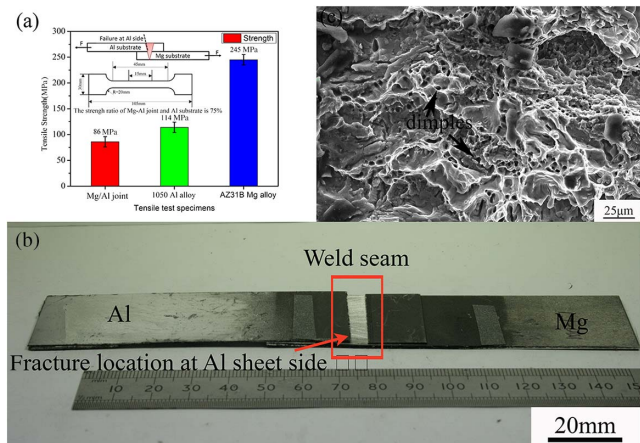Fig. 4. Mg and Al binary phase diagram.

Fig. 5. (a) Tensile shear strength of Mg–Al joints and substrates; (b) Mg–Al specimen after the tensile shear test; (c) an SEM image of the fractured surface.

low and did not solely contribute to the failure of the joint. Furthermore, the Mg–Al interface is composed of fine eutectics structure (Mg solid solution and $Mg_{17}Al_{12}$), which can strengthen the weld. The SEM image of the fractured surface is presented in Fig. 5(c). The appearance of fracture surface is clear evidence of plastic deformation through the presence of a large number of dimples in the matrix alloy and short tearing ridges around the dimples. It can be concluded from the microstructure and fracture toughness that although brittle intermetallics formed around the welded joint, the thickness of the IMC layer was small and in the presence of ductile Mg–Al solid solution around it, a crack formed along the IMC layer that could not propagate freely to cause brittle failure in mechanical testing.

In summary, nanosecond pulsed laser welding of Mg and Al alloys was successfully achieved. The average tensile shear strength of the joints was 86 MPa. The joints fractured toward the Al alloy side rather than at the Mg–Al interface. In the process of joining Mg, vapor filled in the keyhole created by interaction of the laser on the Al substrate. This resulted in formation of solid solution of aluminium in magnesium and intermetallic formation of $Mg_{17}Al_{12}$ at the interface of the joint, resulting in high interfacial strength. The microstructural constituents are correlated to the plasticity observed in the tensile lap shear tests of the joint. Along both sides of the weld seam in aluminium substrate, an extremely thin Mg–Al diffusion zone was formed and analyzed as Mg–Al IMCs. However, because this IMC interlayer was extremely thin and a large proportion of Mg solid solution formed nearby, the toughness of the joint was not affected significantly.

References

1. X. Dai, H. Zhang, H. Zhang, J. Liu, and J. Feng, Mater. Sci. Tech. **32**, 164 (2016).
2. A. Macwan and D. L. Chen, Mater. Sci. Eng. A **666**, 139 (2016).
3. K. Chen, Z. Wang, R. Xiao, and T. Zuo, Chin. Opt. Lett. **4**, 294 (2006).
4. L. M. Liu, H. Y. Wang, and Z. D. Zhang, Scripta Mater. **56**, 473 (2007).
5. M. Sun, S. B. Behravesh, L. Wu, Y. Zhou, and H. Jahed, Fatigue Fract. Eng. Mater. Struct. **40**, 1048 (2017).
6. P. Penner, L. Liu, A. Gerlich, and Y. Zhou, Sci. Technol. Weld. Join. **18**, 541 (2013).
7. N. Yamamoto, J. S. Liao, S. Watanabe, and K. Nakata, J. Jpn. I Met. **73**, 104 (2009).
8. F. Liu, Z. Li, H. Wang, and Y. Bai, J. Mech. Strength **36**, 819 (2014).
9. H. T. Zhang, X. Y. Dai, and J. C. Feng, Mate. Lett. **122**, 49 (2014).
10. J. Shang, K. H. Wang, Q. Zhou, D. K. Zhang, J. Huang, and J. Q. Ge, Trans. Nonferrous Met. Soc. China **22**, 1961 (2012).
11. Y. L. Zhang, F. G. Lu, H. C. Cui, Y. Cai, S. T. Guo, and X. H. Tang, Int. J. Adv. Manuf. Tech. **86**, 2895 (2016).
12. S. Bannour, K. Abderrazak, S. Mattei, J. E. Masse, M. Autric, and H. Mhiri, J. Laser Appl. **25**, 032001 (2013).
13. H. Y. Du, Y. J. Li, G. L. Liu, Y. X. Xu, and J. Wang, Kovove Mater. **53**, 113 (2015).
14. M. Feng, Y. Li, C. Zhao, and Z. Luo, Sci. Technol. Weld. Join. **21**, 688 (2016).
15. L. M. Liu, X. J. Liu, and S. H. Liu, Scripta Mater. **55**, 383 (2006).
16. A. Ascari and A. Fortunato, Opt. Laser Technol. **56**, 25 (2014).
17. C. Luo and L. W. Lin, Sens. Actuat A **97**, 398 (2002).
18. A. W. Alshaer, B. D. Rogers, and L. Li, Comput. Mater. Sci. **127**, 161 (2017).
19. C. Wang, H. Wei, Y. Jiang, J. Wang, Z. Qiao, J. Guo, W. Fan, and X. Li, Chin. Opt. Lett. **14**, 121402 (2016).
20. Q. Wang, L. Jiang, J. Sun, C. Pan, W. Han, G. Wang, H. Zhang, C. P. Grigoropoulos, and Y. Lu, Photon. Res. **5**, 488 (2017).
21. K. Zhang, Z. Lei, X. Wang, Y. Chen, and Y. Zhao, Chin. Opt. Lett. **13**, 061403 (2015).
22. A. Panteli, Y. C. Chen, D. Strong, X. Y. Zhang, and P. B. Prangnell, JOM **64**, 414 (2012).
23. F. Scherm, J. Bezold, and U. Glatzel, Sci. Technol. Weld. Join. **17**, 364 (2013).
24. P. Venkateswaran, Z. H. Xu, X. D. Li, and A. P. Reynolds, J. Mater. Sci. **44**, 4140 (2009).
25. A. Azizi and H. Alimardan, Trans. Nonferrous Met. Soc. China **26**, 85 (2016).